J Mater Sci (2022) 57:1994–2011

Energy materials

Cobalt, nitrogen-doped carbons as catalysts for sodium borohydride hydrolysis: role of surface chemistry

Iryna Ivanenko[1,*] and Anastsiia Ruda[1]

[1] *Department of Inorganic Substances Technology, Water Treatment and General Chemical Engineering of National Technical University of Ukraine "Igor Sikorsky Kyiv Polytechnic Institute", 4 building, 37 Peremohy ave., Kyiv 03056, Ukraine*

Received: 30 July 2021
Accepted: 25 October 2021
Published online: 3 January 2022

ABSTRACT

The development of an effective method for modifying a carbon surface in order to improve its activity and electronic properties for the electrocatalysts creating is a priority task of numerous studies, as well as the current one. This study describes an attempt to modify the surface of traditional porous carbon support in several ways, for the further increment of cobalt, in order to create a highly active and stable catalyst for the hydrolysis of sodium borohydride. Two series of cobalt- and/or nitrogen-doped catalysts were prepared by the impregnating of pre-oxidized industrial active carbon. These were: two catalysts with 10 and 20% of cobalt content based on the oxidized active carbon, as well as two catalysts with 10 and 20% of cobalt content based on the nitrided oxidized active carbon. The presence of cobalt in all the doped samples was confirmed by both X-ray phase and X-ray structural analysis. It was found that the oxidation, nitriding, and doping with cobalt lead to the consistent decrease in the surface area and the total porosity; however, it did not affect their catalytic activity. The largest H_2 volumes at temperatures of 60, 70, and 80 °C and hydrogen generation rates of 1667, 2857, and 5000 mL/(g_{cat}·min), respectively, were found in the presence of the catalyst doped with nitrogen and cobalt, with the content of the latter of 10%; the activation energy constituted 41 kJ/mole. The study of the surface chemistry of the catalysts by the two methods (pH-potentiometric titration, and adsorption of Hammett indicators from an aqueous medium) made it possible to explain the mechanism of cobalt attachment and to determine the possible forms of its existence on the surface of the oxidized and nitrided oxidized activated carbon matrix.

Handling Editor: Joshua Tong.

Address correspondence to E-mail: irinaivanenko@hotmail.com
E-mail Address: nastenaru@ukr.net

https://doi.org/10.1007/s10853-021-06663-x

Introduction

Hydrogen electrical devices are environmentally friendly and nonpolluting, and reduce greenhouse gas emissions, making us less dependent on fossil fuels. However, those devices are not yet economically viable, and current hydrogen production depends on natural gas. If we can develop a process to economically produce hydrogen in an environmentally sound way, fuel-cell devices may be the way for the future.

Hydrolysis of borohydride is one of the most important reactions due to its widespread application and the demand for practical need in fuel cells and metal-air power sources [1]. Noble metals deposited on porous matrixes are widely used as a catalytic material for the reaction of oxygen reduction in general [1–5] and borohydride hydrolysis in particular [6–9]. Great strides have also been achieved in the development of non-noble metals catalytic systems. For example, cobalt [10–12], nickel [13–15], iron [16–18], copper [19], manganese [20, 21], mixed catalysts [22–26] and many other metals.

The main reason that leads to the corrosion of metallic deposited catalysts is related to the degradation of the support. It causes the destruction of the porous structure, thus preventing the mass transfer of reagents toward the active centers and initiating the detachment of metal nanoparticles. The enlargement of their particles also takes place due to agglomeration and Ostwald ripening, which causes the following reduction of the electrochemically active surface area of metallic deposited catalysts [27].

Supporting materials have a significant impact on the productivity and durability of the catalyst, and hence the entire cost of the fuel cell systems. Among effective support materials, there are many different ones: multi-walled carbon nanotubes [27, 28], carbon nanospheres [29, 30], zeolite [31, 32], bentonite clays [33], graphene [3, 34], graphene oxide [35], carbon cloth [36], sometimes completely new matters occur, such as bacterial cellulose derived carbon [37], superporous p(AAc (acrylic acid)) cryogels [38], macroscopic biopolymer hydrogel [39], unexpected honeycomb matrix [40] and honeycomb ceramic monolith [41], as well as many others.

The material, as a catalyst carrier, must possess a large specific surface area and a predominantly mesoporous structure for reagents transporting. It must also have high stability in alkaline and acidic environments under the operating conditions of fuel cells. As the electrically conductive support material provides a pathway for the electron transfer between the support and the deposited metal, it must possess high proton and electronic conductivity. In order to increase the stability of the catalyst, strong interaction must be provided between the nanoparticles of the metal and support material.

Activated carbon entirely meets all of the mentioned above requirements. However, the relatively inert surface of the initial activated carbon does not allow the reliable attachment of metal nanoparticles, due to an insignificant number of active centers on its surface.

Among the well-spread approaches for the formation of surface-active sites, the two main ones can be distinguished. The first approach consists in the creation of oxygen-containing functional groups [27, 42] and the second one implements due to the introduction of heteroatoms such as N, P, B, and S into a system of condensed aromatic rings of active carbon [8, 11, 14, 17, 18, 24, 25, 27, 31, 33, 34, 36, 37, 41, 43].

The presence of heteroatoms in the carbon structure provides the altered electronically enriched structure of the carbon matrix, increases the strength of the subsequent bond of the introducing metal with the support, thus, as a result, leads to the increasing of the stability of the entire system [27, 44–46]. Moreover, the larger the number of active centers the smaller the size of the introduced metal particles and the stronger their bond with the support. All this facilitates charge transfer, thereby increasing the catalytic activity of non-noble metals deposited on porous carbon [27, 44–46].

The development of an effective method for modifying a carbon surface in order to improve its activity and electronic properties is a priority task of numerous studies, as well as the current one. It might be crucial when creating electrocatalysts.

This study describes an attempt to modify the surface of traditional porous carbon support in several ways, for the further increment of cobalt, in order to create a highly active and stable catalyst for the hydrolysis of sodium borohydride.

Materials and methods

The catalysts synthesis

Norit SAE Super activated carbon was used as the initial material (AC_{in}). It was treated with boiling nitric acid (1:1) for 1 h to obtain the oxidized active carbon (AC_{ox}). Then, some part of AC_{ox} was modified with nitrogen through the melamine impregnation method [43] for obtaining the nitrided oxidized active carbon (N/AC_{ox}). For this 20 g of AC_{ox} and 5 g of melamine were dissolved in distilled water, stirred at room temperature, heated until the liquid was evaporated, dried, and calcined at 850 °C in an inert atmosphere.

The oxidized active carbons doped with metallic cobalt were also prepared: $Co(10)/AC_{ox}$ contained 10 wt.% of cobalt, as well as $Co(20)/AC_{ox}$ contained 20 wt.% of cobalt. In the synthesis process, the AC_{ox} was dispersed in alcohol using ultrasonication, the necessary amount of cobalt nitrate was added there and dissolved by stirring, and solute oxygen was displaced from the flask by the flowing inert gas. The obtained suspension was heated to 70°C in a water bath and a hydrazine alkaline solution was added drop by drop with careful stirring. The hydrazine hydrate served as a classical energetic reducing agent in order to prevent the oxidation of cobalt to its oxides. After that the suspension was stirred at 70 °C in a water bath additionally during an hour; the obtained precipitate was washed with alcohol by magnetic decantation and dried.

The samples of $Co(10),N/AC_{ox}$ and $Co(20),N/AC_{ox}$ were derived with a combination of the last two methods. The cobalt contents were exactly 10% and 20% in all final catalysts, which was checked and proved by their thermogravimetric analysis.

Catalysts characterization

In order to obtain direct, accurate, and reliable information about the phase composition and structure of synthesized catalysts samples X-ray phase analysis (XRD) was performed on a universal X-ray diffractometer Rugaku Ultima IV in copper Cu Kα radiation (λ = 0.154184 nm) at a rate of 2 deg/min.

Structurally adsorptive characteristics of the catalysts, such as specific surface area (S_{sp}, m^2/g) and total pores volume ($V_{\sum}$, cm^3/g), were determined by a static method through adsorption of benzene vapors under the ambient conditions.

The pH-potentiometric titration method was used to investigate the ion-exchange properties of the surface and the point of zero charge (pzc) of the synthesized catalysts. A weighted mass (0,1 g) of each sample was dispersed in 25 mL of 0,2 M sodium chloride aqueous solution, as well as 0,1 M of NaOH (or 0,1 M HCl) were added in each of twelve flasks in order to create the required pH. In order to make the total fluid volume of 50 mL, the distilled water was added to each flask. The flasks were shaken for 4 h, and after that, the pH of each solution was determined. At the same time, an "empty" trial was performed; it was similar to the previous one but without a catalyst sample. The graphical dependence of solution pH on the volume of NaOH (or HCl) added was constructed on the basis of the obtained data. The pzc was determined as the intersection point of the graphs of "empty" solution and solution with the catalysts sample in each experiment.

The difference between the abscissas of the two points lying on the different titration curves, at the same pH value, allowed to calculate the number of millimoles of H^+-ions which were displaced from the catalyst at a given pH, namely the value a^+ (mmol/g) and a^- (mmol/g):

$$a^{+/-} = C_{ac/alk} \cdot (V_1 - V_o)/m \quad (1)$$

$C_{ac/alk}$ is the initial concentration of the acid (alkali) solution, mmol/mL;

V_1 is the volume of the acid (alkali) solution with the catalyst at definite pH, mL;

V_o is the volume of the acid (alkali) solution without the catalyst at definite pH, mL; m is the mass of catalysts, g.

The acid–base properties of the catalysts' surface were determined by the method of adsorption of Hammett indicators from an aqueous medium. The thirteen indicators with pK_a values from + 0.80 to + 12.8 were used for this purpose, and their concentrations before and after the interaction with the catalysts were determined by the photocolorimetric method. The list and the characteristics of the catalysts used are presented in Table 1.

Table 1 Characteristics of the acid–base indicators used

	Indicator	pKa	λ_{max}, нм
1	Crystal violet	+ 0,80	580
2	Diamond green	+ 1,30	610
3	Methyl orange	+ 3,46	460
4	Bromophenol blue	+ 4,10	590
5	Methyl red	+ 5,00	430
6	Chrysoidin	+ 5,50	448
7	Bromocresol purple	+ 6,40	540
8	p-Nitrophenol	+ 7,15	360
9	Bromothymol blue	+ 7,30	430
10	Thymol blue	+ 8,80	430
11	Pyrocatechol	+ 9,45	274
12	Tropeolin 00	+ 12,00	440
13	Indigo carmine	+ 12,8	610

The catalytic test

The catalytic properties of the synthesized catalysts samples were investigated on the sealed volumometric installation. The sample of the tested catalyst (0,01 g) and sodium borohydride (0,1 g) was placed in the reactor with the water jacket and the portion of distilled water (15 cm^3) was added. The gas supplanted during the reaction displaced the water to the cylinder and thus the amount of the released hydrogen was controlled. The reaction of sodium borohydride hydrolysis was performed with each sample at room temperature which was 17 °C. The catalytic tests were carried out at temperatures 60, 70, and 80°C for activation energy determination as well. The hydrolysis reaction of sodium borohydride is described by the equation: $NaBH_4 + 2H_2O \rightarrow 4H_2\uparrow + NaBO_2$.

The current concentration of sodium borohydride was calculated based on the volume of released hydrogen, and the order of the catalytic reaction was determined. The rate constant (k, c^{-1}) of the catalytic reaction of $NaBH_4$ hydrolysis was calculated by the formula (2) for the first-order reaction:

$$k = \frac{1}{\tau}\ln\frac{C_0}{C_\tau} \quad (2)$$

C_o and C_τ is the initial and current concentration of sodium borohydride, respectively, at the current time (τ, sec).

Also, k was calculated by using the half-life ($\tau_{½}$) that is the time during which the initial $NaBH_4$ concentration was halved, according to the formula (3):

$$k = \frac{\ln 2}{\tau_{1/2}} \quad (3)$$

The formula (4) was used for the analytical definition of the activation energy of the investigated catalytic reaction (E_a, kJ/mole):

$$E_A = \frac{RT_1T_2ln\frac{k_2}{k_1}}{T_2 - T_1} \quad (4)$$

Results and discussion

X-ray phase analysis and internal surface

The crystal structure of the initial active carbon and the synthesized catalysts were characterized by X-ray diffraction; XRD patterns are presented in Fig. 1.

As it can be seen in Fig. 1a, the initial active carbon (AC_{in}) was X-ray amorphous and it manifested only one blurry maximum at 2θ with width from 19.5° to 29.5°. The plans of carbon were located in this range, according to the ICDD Standard Card №00–022-1069: (110) at 19.85°, (111) at 20.83°, (201) at 23.97°, (104) at 27.68°, and (203) at 29.45°. The oxidized carbon (AC_{ox}) showed the similar diffraction pattern, although the intensity of the mentioned above peak increased by 20%. This peak was also presented in the diffraction pattern of the nitrided oxidized carbon (N/AC_{ox}). Besides that N/AC_{ox} showed the blurry maximum at 2θ from 39.5° to 48.5° as well. In this range, the planes of carbon (205) at 39.49°, (220) at 40.22°, (304) at 43.04°, and (305) at 47.57° were detected, according to the ICDD Standard Card №00–022-1069.

After doping with cobalt, several relatively intense peaks appeared in the diffraction pattern of the X-ray amorphous oxidized active carbon, as it can be seen in Fig. 1b. Namely, there were peaks at 2θ values of 32.5° (210), 38.4° (301), 40.5° (114), 51.2° (222), 58.2° (501), 64.5° (530), 69.8° (432), and all of them belonged to cobalt according to the ICDD Standard Card №01–078-4003. In the spectra of $Co(10)/AC_{ox}$ and $Co(20)/AC_{ox}$ catalysts (see Fig. 1b), there occurred many indistinct maximums of carbon in the range of 2θ from 19.5° to 29.5°, and several distinct peaks of cobalt of low-intensity occurred as well, for instance:

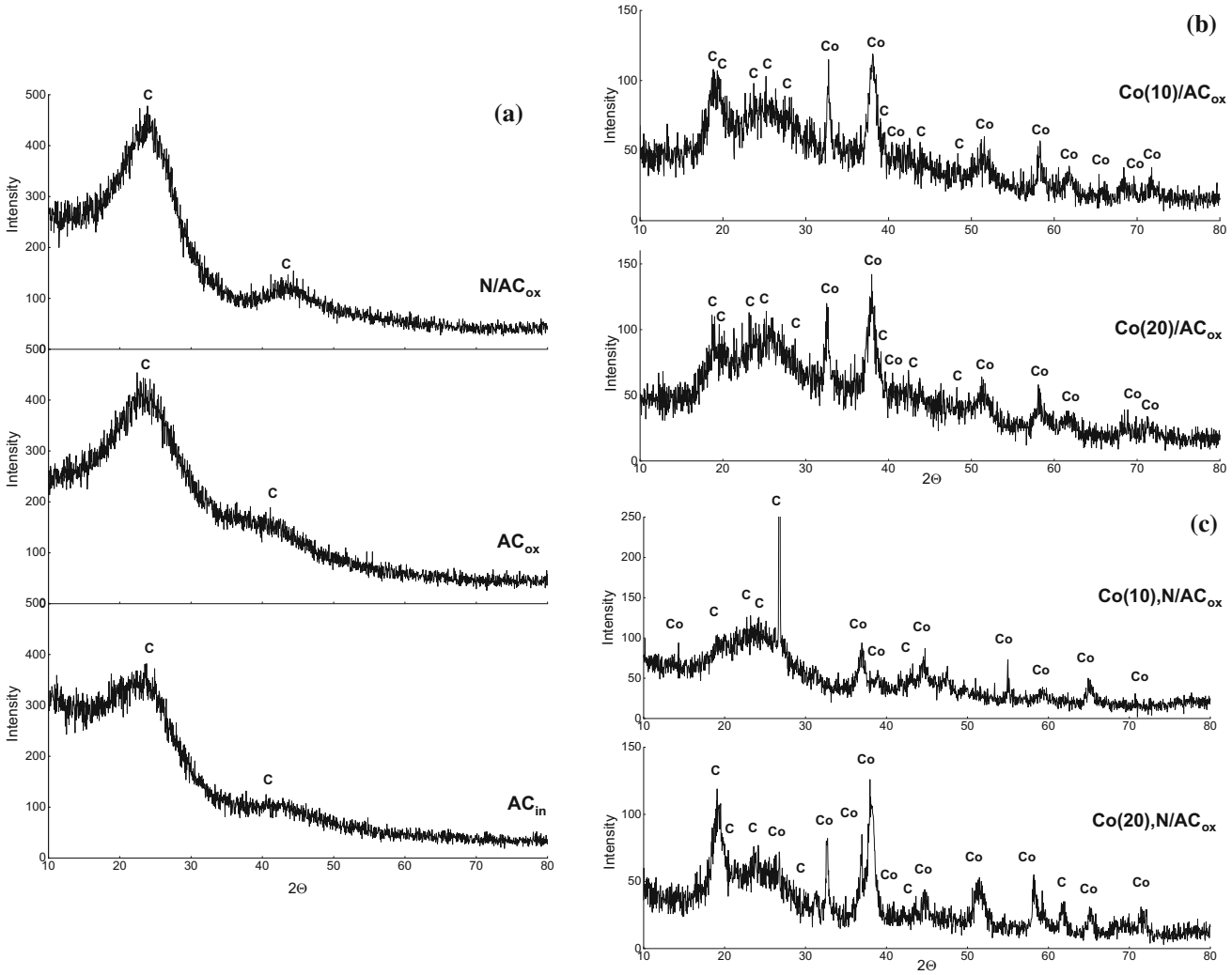

Figure 1 XRD pattern of **a** the initial, oxidized, and nitrided oxidized active carbons; **b** oxidized active carbons doped with cobalt in 10 and 20%; and **c** nitrided oxidized active carbons doped with cobalt in 10 and 20%.

20.8° (102), 24.5° (200), 27.3° (112), 30.1° (202) according to the ICDD Standard Card №01–078-4003.

In the XRD pattern of the nitrided oxidized active carbons doped with cobalt (Fig. 1c), several peaks which were attributed to cobalt were presented. However, the diffraction patterns of Fig. 1c showed that cobalt in these two composites crystallizes in different ways.

In the sample Co(10),N/AC$_{ox}$, the maxima at 2θ = 37.6°, 38.9°, 43.2°, 44.4°, 47.5°, 49.2°, 51.1°, 53.3°, and 57.1° of the planes (301), (311), (112), (410), (212), (411), (222), (312), and (322), respectively, were clearly visible (according to the ICDD Standard Card №01–078-4003). Its most intensive peak at 26.5° belonged to carbon (see Fig. 1c). As is generally accepted, a higher intensity and narrower width of C (002) at 26.5° peak mean a higher degree of graphitization and the larger the crystal size of carbon [47–49].

Table 2 Structural adsorption characteristics of the catalysts

Catalysts	S_{sp}, m^2/g	$V_{\sum}$, cm^3/g
AC$_{in}$	1150	0,78
AC$_{ox}$	640	0,45
Co(10)/AC$_{ox}$	510	0,25
Co(20)/AC$_{ox}$	495	0,21
N/AC$_{ox}$	350	0,13
Co(10),N/AC$_{ox}$	345	0,12
Co(20),N/AC$_{ox}$	340	0,12

In the sample Co(20),N/AC_{ox}, the planes (211), (210), (221), (301), (410), (330), (331), (222), (430), (501), (511), (412), (422), (313) with peaks at 2θ = 31.1°, 32.7°, 36.7°, 37.9°, 44.5°, 45.3°, 50.5°, 51.2°, 54.6°, 58.2°, 59.3°, 61.6°, 65.0°, 72.0°, respectively, were crystallized (according to the ICDD Standard Cards №01–078-4003 and №01–070-2633) (see Fig. 1c).

Structural adsorption characteristics of the synthesized samples of the catalysts are shown in Table 2. The initial active carbon possessed 1150 m^2/g of surface area and 0.78 cm^3/g of total porosity; they were the largest values among the studied catalysts. Its specific surface area and porosity decreased by half to 640 m^2/g and 0.45 cm^3/g, respectively, after the treatment with boiling nitric acid. In our opinion, the destruction of the active carbon structure occurred because boiling nitrate acid, as a strong oxidizing agent, chemically interacted with the peripheral carbon atoms of activated carbon to produce humic acids. As a result of this interaction, the external channels (macropores) of active carbon were destroyed and eroded. This led to a significant reduction in the structural characteristics of the AC, as the share of macropores in the total porosity and specific surface area is very large. Despite the fact that there are found many different, sometimes contradictory opinions on the topic of oxidized carbons, the authors of [50, 51] hold a similar point of view.

The nitriding of the oxidized carbon surface led to the consequent reduction of surface areas by half, and to the reduction of total porosity by three. Melamine, as an organic base, had formed complex salts with

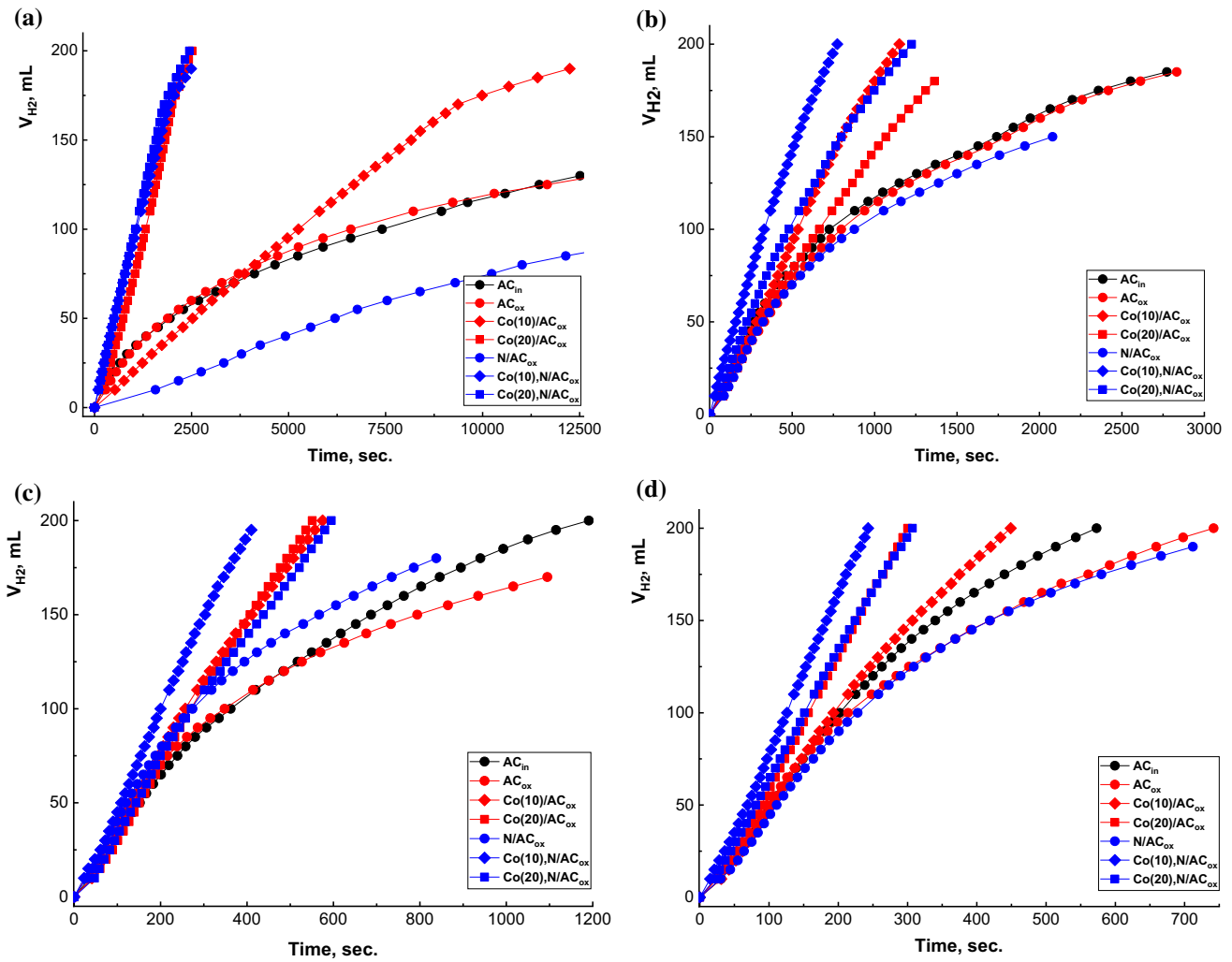

Figure 2 Hydrogen released from $NaBH_4$ solution in the presence of the synthesized catalysts at temperatures: 17 °C **a**, 60 °C **b**, 70 °C **c**, and 80 °C **d**.

Table 3 HGR measured in the presence of catalysts tested at different temperatures

Catalysts	HGR (mL/(g_{cat}· min)) at temperatures:			
	17 °C	60 °C	70 °C	80 °C
AC_{in}	41	402	1052	2230
AC_{ox}	38	394	944	1666
$Co(10)/AC_{ox}$	103	1052	2222	2857
$Co(20)/AC_{ox}$	561	818	2222	4000
N/AC_{ox}	32	441	1385	1727
$Co(10),N/AC_{ox}$	512	1667	2857	5000
$Co(20),N/AC_{ox}$	575	1000	2222	4000

acidic functional groups of the active carbon, which decomposed when further heated. Probably, during the heating of the suspension of active carbon and melamine, drying, and calcination at 850 °C of precipitate, a certain part of the formed complex salts was washed out, decomposed, and flies away, destroying the outer macropores. The loss of mass during calcination also took place. As a result, not only the porosity decreases, but also the specific surface area.

The specific surface area and porosity of the oxidized active carbon and the nitrided oxidized active carbon continued to decrease after doping with cobalt. The smallest structural adsorption characteristics corresponded to $Co(10),N/AC_{ox}$, and $Co(20),N/AC_{ox}$ catalysts.

Catalytic tests

Figure 2 shows the results of the catalytic activity tests of the initial, oxidized, and nitrided oxidized active carbons as well as the oxidized active carbons doped with cobalt in 10 and 20%; and the nitrided oxidized active carbons doped with cobalt in 10 and 20% at four different temperatures.

It was observed that with the temperature rising, the rate of hydrolysis of sodium borohydride strongly increased; the initial, oxidized, and the nitrided oxidized active carbons which were not doped with cobalt have demonstrated the lowest catalytic activity. The biggest hydrogen volume was released in the presence of active carbon catalysts doped with cobalt, which was fully expected. Table 3 illustrates the hydrogen generation rate (HGR, mL/(g_{cat}· min)) measured in all the performed catalytic tests.

As it can be seen in Table 3, the maximum of HGR at room temperature was achieved in the presence of $Co(20),N/AC_{ox}$ catalyst: it was 575 mL/(g_{cat}·min). 230 mL of H_2 were released at the $NaBH_4$ hydrolysis of the initial concentration of 0.7 wt.%, in the presence of 0.01 g catalyst during 40 min. The highest values of HGR at all the three other investigated temperatures have been discovered for $Co(10),N/AC_{ox}$ catalyst: 1667, 2857, and 5000 mL/(g_{cat}·min). Those values were achieved during 12; 7; and 4 min, respectively, through the $NaBH_4$ hydrolysis of 0.7 wt.% in the presence of 0.01 g catalyst.

These experimental results are consistent with the known published ones [11, 52–61], as well as confirm the competitively high catalytic activity of the synthesized cobalt-doped carbon catalysts.

In order to determine the order of the reaction and calculate the activation energy, the analysis of experimental data was additionally performed. Graphical dependences of the current concentration of sodium borohydride on the reaction time were not rectilinear; thus, the zero order was excluded. In order to check the first order of the reaction, the graphical dependences of the natural logarithm of the $NaBH_4$ current concentration on the reaction time, at the investigated temperatures were built, as shown in Fig. 3. All the obtained dependences were rectilinear; the maximum square deviation from the linearity did not exceed 0.6%, which corresponded to the error limits. Thus, the first order of the reaction of catalytic hydrolysis of sodium borohydride under the studied conditions was confirmed.

The activation energy (E_a) of the investigated catalytic reaction was determined by the graphical method. Figure 4a shows the Arrhenius plot of ln(k) versus 1/T for all the catalysts. On the basis of the slope of the approximated straight line, E_a for $NaBH_4$ hydrolysis in the presence of the obtained catalysts was calculated.

E_a was calculated by the formula (4) as well. The error of determination by both methods did not exceed 1,5%. The results of those calculations in the form of a histogram of the Activation energy averaged values are shown in Fig. 4b.

As it is seen in Fig. 4b, the lowest activation energy (40 kJ/mole) was observed in the presence of the $Co(10)/AC_{ox}$ catalyst. The value close to it (41 kJ/mole) corresponded to the most active catalyst, namely $Co(10),N/AC_{ox}$. The low value of E_a (44 kJ/mole) was also observed in the reaction

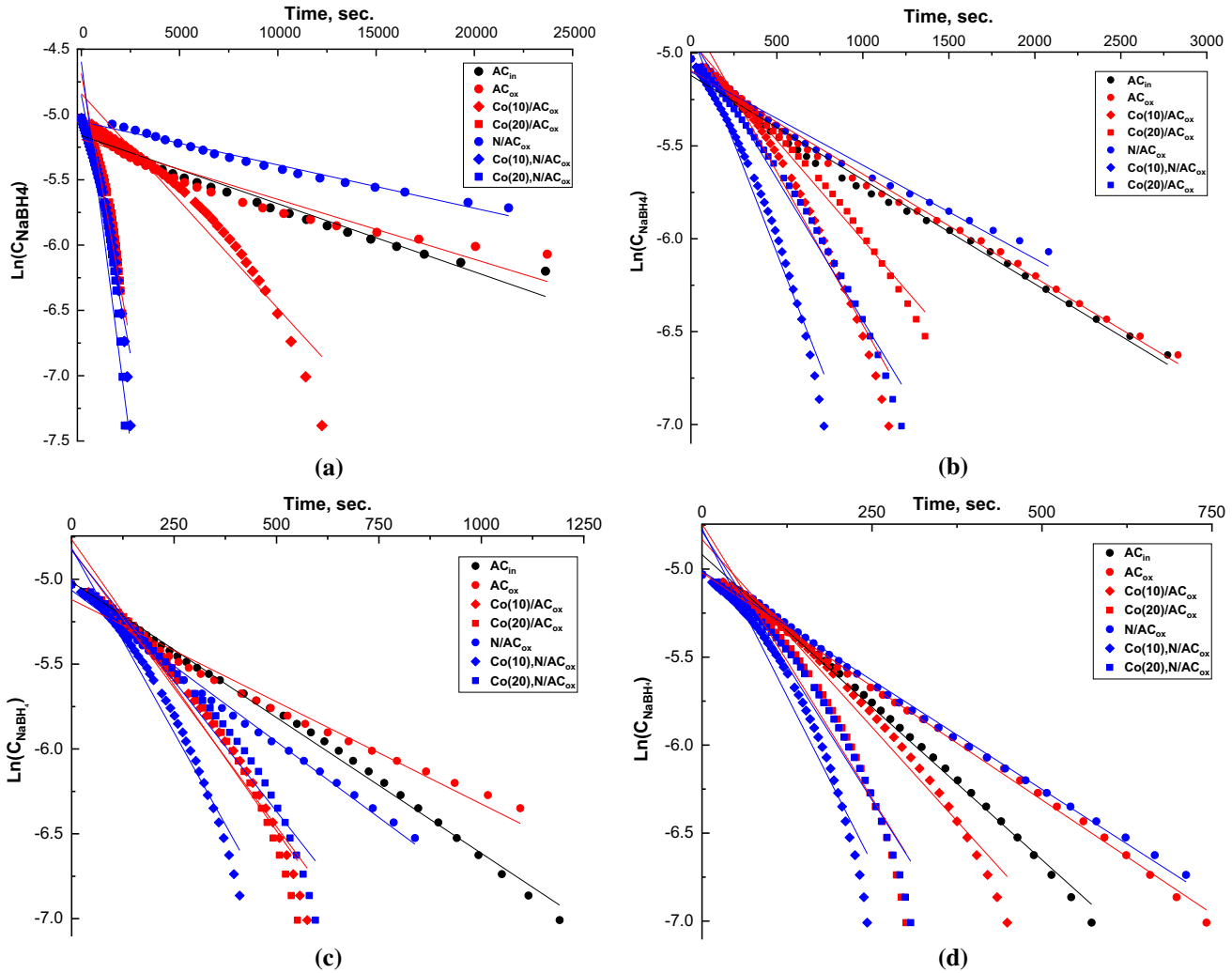

Figure 3 Dependence of the logarithm of the $NaBH_4$ current concentration on the reaction time carried out at temperatures: 17 °C **a**, 60 °C **b**, 70 °C **c**, and 80 °C **d**.

realized with Co(20),N/AC_{ox}. It is important to underline that in the presence of one of the least active catalysts, namely N/AC_{ox}, the activation energy of the reaction was comparatively low (45 kJ/mole), and vice versa, with one of the most active catalysts, Co(20)/AC_{ox}, E_a was high (47 kJ/mole).

The obtained values of the activation energy of $NaBH_4$ hydrolysis were in complete agreement with the previously reported results; they could compete with some of them as well [11, 52–61].

In order to explain such a difference in the behavior of the synthesized catalysts in the $NaBH_4$ hydrolysis reaction, as well as to elucidate its mechanisms, surface chemistry was investigated.

Surface chemistry

The ion-exchange properties of the surface and the point of zero charge (pzc) of the synthesized catalysts were determined by the pH-potentiometric titration method; the obtained results are presented in Table 4.

It can be seen in Table 4 that the initial activated carbon (AC_{in}) showed a low cation exchange capacity (only 0.3 mmol/g) in the pH range: from 3.1 to 4.0. The point of zero charge of the AC_{in} came at pH 4.0. Anion exchange on the surface of the initial activated carbon occurred in a wide pH range: from 4.0 to 11.6. The maximal anion exchange capacity of the AC_{in} was 1.1 mmol/g. This was due to the peculiarities of the obtaining technology of this type of activated carbon, as well as to its alkaline reaction.

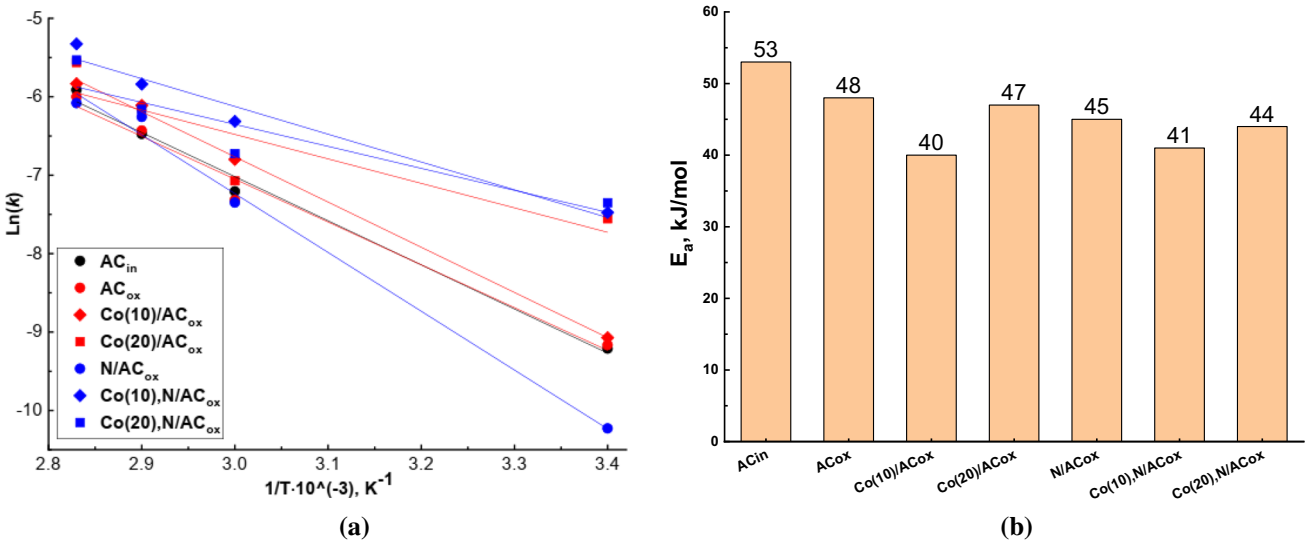

Figure 4 Arrhenius plot of ln(k) versus 1/T **a** and Activation energy **b** of $NaBH_4$ hydrolysis reaction in the presence of the synthesized catalysts.

Table 4 Ion-exchange properties of the catalysts

Catalysts	pH range of cation exchange	a^+, mmol/g	pH_{pzc}	pH range of anion exchange	a^-, mmol/g
AC_{in}	3.1–4.0	0.3	4.0	4.0–11.6	1.1
AC_{ox}	3.0–9.5	3.2	–	–	–
$Co(10)/AC_{ox}$	7.1–10.2	2.0	10.3	10.3–11.7	0.8
$Co(20)/AC_{ox}$	6.8–10.2	2.0	10.3	10.3–11.7	1.0
N/AC_{ox}	3.2–11.4	0.4	11.4	11.4–11.7	0.3
$Co(10),N/AC_{ox}$	3.3–11.0	0.9	11.0	11.0–11.8	0.5
$Co(20),N/AC_{ox}$	7.3–11.0	1.5	11.0	11.0–11.8	0.5

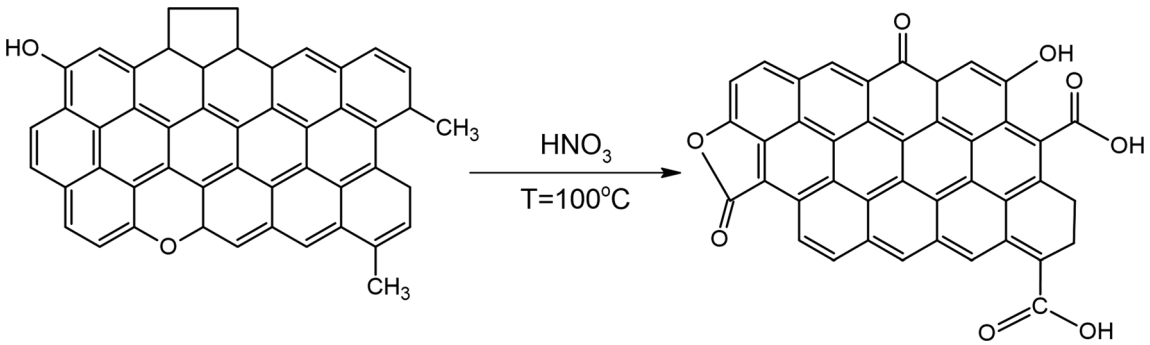

Figure 5 Schematic presentation of the oxidizing of initial active carbon surface by nitric acid.

The oxidized activated carbon (AC_{ox}) showed high cation exchange properties in a wide pH range: from 3.0 to 9.5; it did not show anion exchange capacity at all; therefore, AC_{ox} did not have the pzc. The maximal cation exchange capacity recorded for the oxidized activated carbon constituted 3.2 mmol/g (see Table 4). Such data completely confirmed the presence of the acidic surface functional groups (carboxylic, phenolic, lactone, and their combinations) on the carbon surface, which were formed during the oxidation by nitric acid, as well as the complete absence of the groups capable of anion exchange. The

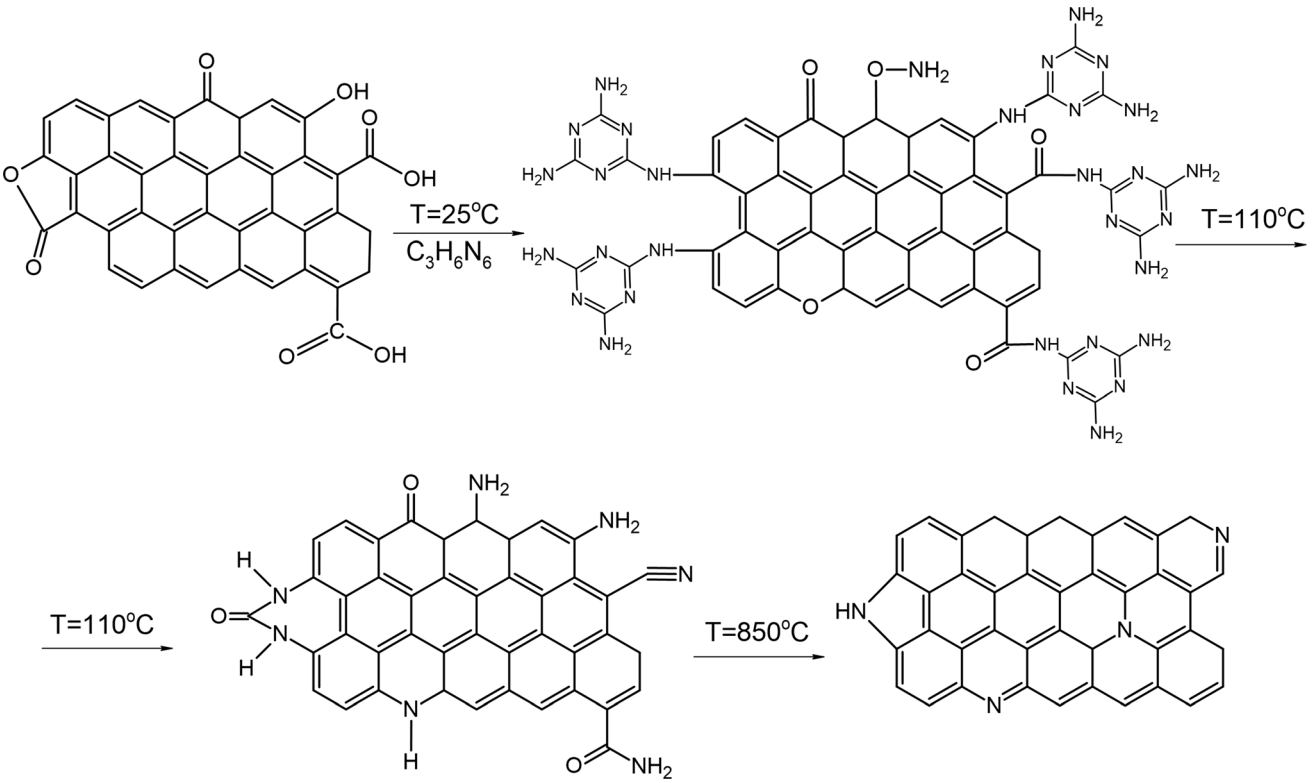

Figure 6 Schematic presentation of the interaction of the oxidized active carbon surface with melamine.

chemical transformations that occur on the surface of the initial activated carbon during its treatment with boiling nitric acid can be very approximately depicted, as it is shown in Fig. 5.

The introduction of the metallic cobalt (in the amount of 10 and 20%) in the matrix of the oxidized carbon had led to the narrowing of the range of cation exchange and to the decrease in cation exchange capacity, as well as to the appearance of the anion exchange ability and, consequently, to the pzc at pH 10.3 (see Table 4). These data indicated to the fact that cobalt atoms were attached to the surface of active carbon through the side functional groups, by the exchange reaction with their H^+-ions, and confirmed the covalent nature of the chemical bond between the introduced cobalt and the oxidized carbon surface.

After the insertion of nitrogen into the oxidized carbon matrix, the range of cation exchange greatly expanded and shifted toward more alkaline pH, however, the cation exchange capacity of the nitrided oxidized active carbon (N/AC_{ox}), remained not very high (0.4 mmol/g). Anion exchange on the surface of the nitrided oxidized active carbon occurred in the very narrow pH range: from 11.4 to 11.7, and its point of zero charge was at pH 11.4 (see Table 4).

The multifunctional nature of the surface of the nitrided oxidized active carbon, in our opinion, is explained as follows: in the process of the impregnating of the oxidized active carbon with melamine and subsequent calcination, first, the complete destruction of the outward oxygen-containing functional groups occurs, and then the formation of the new, but already nitrogen-containing groups [42] originates (Fig. 6). The newly formed pyridine, pyridine N-oxide, pyridone, and pyrrole are able to generate the corresponding cations and anions in aqueous solutions, as it will be shown below.

After the insertion of cobalt into the nitrided oxidized carbon matrix, its acidity increased and the basicity practically did not change. The catalyst with a lower content of cobalt ($Co(10),N/AC_{ox}$) exhibited the cation exchange capacity in the pH range: from 3.3 to 11.0. The maximum cation exchange capacity constituted 0.9 mmol/g, and the point of zero charge was at pH 11.0. The anion exchange properties of $Co(10),N/AC_{ox}$ were exhibited in the very narrow pH range: from 11.0 to 11.8, the maximum of its anion exchange capacity was 0.5 mmol/g. The catalyst with more content of cobalt ($Co(20),N/AC_{ox}$) showed the higher cation exchange capacity, which constituted

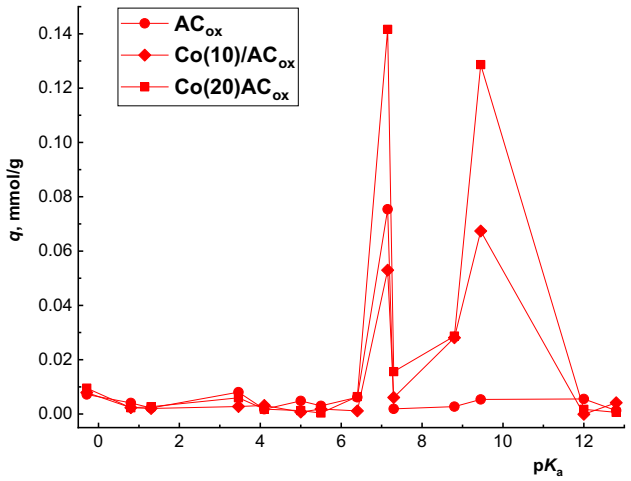

Figure 7 Acid–base sites on the surface of the oxidized active carbon and of cobalt-doped catalysts obtained on its basis.

1.5 mmol/g, but it was active in the narrow pH range: from 7.3 to 11.0. The point of zero charge was also at pH 11.0. Anion exchange properties were manifested in the similar narrow range of pH: from 11.0 to 11.8, and the maximum of its anion exchange capacity constituted also 0.5 mmol/g.

Thus, the introduction of less amount of cobalt (with the same initial nitrogen content) widened the range of cation exchange more significantly and promoted the increase in the cation exchange capacity, but did not affect the exchange of anions at all. Such experimental data allowed to assume the formation of various and different surface groups and complexes, the nature of which was very strongly dependent on the content of the doping metal.

In order to confirm this hypothesis, as well as to clarify the mechanism of cobalt attachment and to determine the possible forms of its existence on the surface of the initial, oxidized, and nitrided oxidized carbon matrix, the investigation of the synthesized catalysts by the method of adsorption of Hammett indicators from an aqueous medium was performed.

As it is seen in Fig. 7, there was the only maximum at pK_a = 7.15 on the surface of the active carbon oxidized with nitric acid. Since strong acids (carboxylic) have pK_a below 8 and weak acids (phenols) have pK_a over 8, as discussed by Teresa J. Bandosz [62], it was concluded that the both types of surface centers were presented and caused the single peak appearance in the neutral region.

After the introduction of cobalt into the oxidized carbon matrix, the intensity of the peak at pK_a = 7.15 changed: it almost doubled for the Co(20)/AC$_{ox}$ catalyst and decreased by a quarter for the Co(10)/AC$_{ox}$ catalyst (Fig. 7). Such changes, in our opinion, were explained by the chemical interaction of surface carboxyl and phenolic groups with cobalt, as a result of which, cations of the corresponding salts of carboxylic acids and phenolates were formed, as it is shown in Fig. 8a. The inserted cobalt in the amount of 10% was not enough to interact with all O-containing surface groups; therefore, the intensity of the pK_a = 7.15 maximum decreased for the Co(10)/AC$_{ox}$ catalyst. On the contrary, 20% of the introduced cobalt in the Co(20)/AC$_{ox}$ catalyst was sufficient for the complete neutralization of acids (carboxyl and phenols), as well as for the formation of an additional amount of Co^+-cations, trapped between the carbon graphitized planes (see Fig. 7).

The emergence of the new peak at pK_a = 9.45 was observed which did not take place until the introduction of cobalt (see Fig. 7). According to our supposition, its appearance is caused by the fact that the formed cations of salts of carboxylic acids and phenolates, being in aqueous solutions, attract OH^--groups very easily, and the H^+-cations are produced

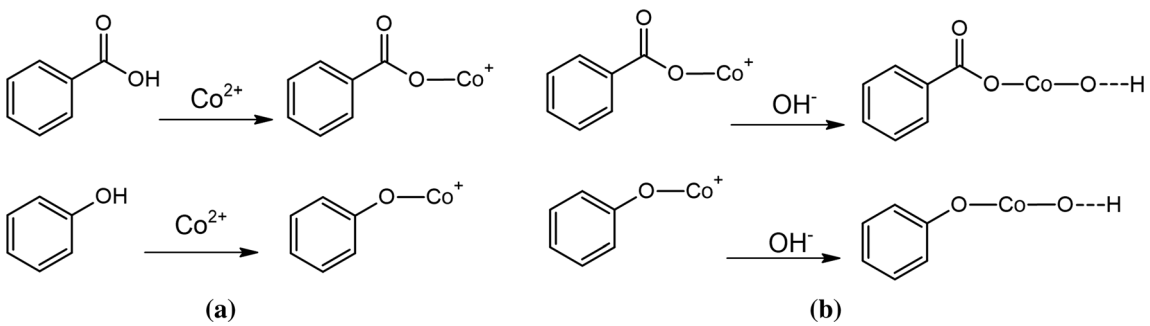

Figure 8 Chemical interaction of the surface carboxyl and phenolic groups with cobalt **a**, and H^+-cation generating as a result of the attraction of OH^--groups by the formed cations of salts of carboxylic acids and phenolates **b**.

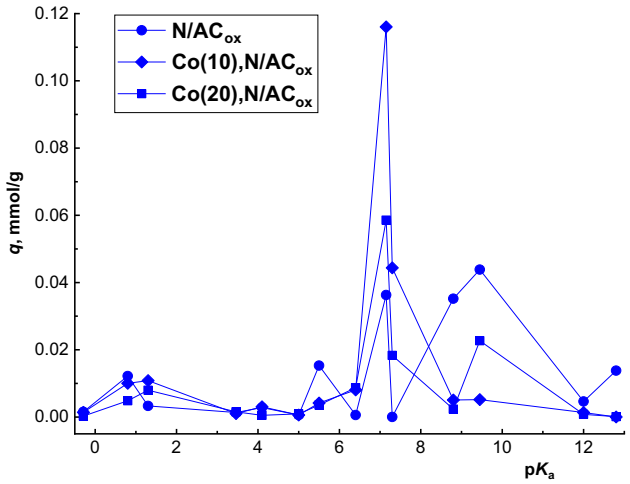

Figure 9 Acid–base centers on the surface of nitrided oxidized active carbon and of the cobalt-doped catalysts obtained on its basis.

as a result. These transformations can be depicted very conditionally as in Fig. 8b.

The results of the determination of acid–base centers on surface of the nitrided oxidized active carbon and the cobalt-doped catalysts obtained on its basis are presented in Fig. 9.

The small maximum at pK_a = 0.8 (see Fig. 9) belonged to pyridine N-oxide, which is known as Lewis base. However, the canonical forms, in which oxygen is neutral and the pyridine ring is negatively charged, make a significant contribution to the structure of pyridine N-oxide. In the reality, the situation is even more delicate, since the resonance forms carrying the positive charge at the α- and γ-positions also suppose the existence of the opposite polarization of the cycle, as it is shown in Fig. 10. Therefore, the N-oxide group in pyridine N-oxides facilitates the nucleophilic and electrophilic substitution reactions at these positions, depending on the conditions.

The participation of cobalt in nucleophilic and electrophilic substitution reactions with pyridine N-oxide is thermodynamically impossible. Therefore, pyridine N-oxide did not undergo any changes during doping with cobalt, except for the opposite polarization of the cycle, which did not affect the total acidity of these centers. As a result, the low maximum at pK_a = 0.8 remained after doping with cobalt (see Fig. 9).

It is well known, that quaternary nitrogen belonging and being covalently bonded to three adjacent rings, contains a positively charged nitrogen atom. Therefore, quaternary nitrogen, being weak Bronsted acid, caused the peak at pK_a = 5.5 (see Fig. 9). Its complete disappearance after the introduction of cobalt can be explained by two reasons. First, donor–acceptor surface complexes were formed, in which the π-electrons of the nitrogen atom were displaced to the vacant orbitals of cobalt ions. Second: the chemical bonding of one cobalt atom by quaternary nitrogen atoms, located in different graphitized

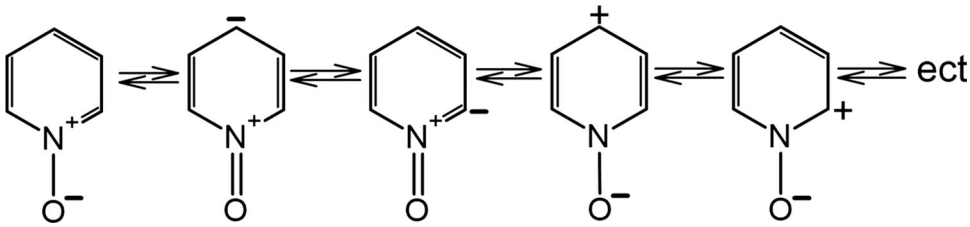

Figure 10 The opposite polarization of the pyridine N-oxide cycle due to the resonance forms with positive charge at the α- and γ-positions.

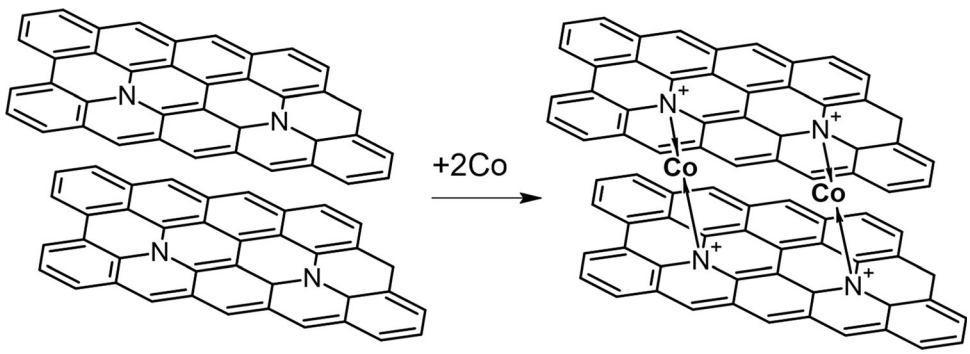

Figure 11 Chemical bonding of cobalt by quaternary nitrogen atoms of different graphitized planes.

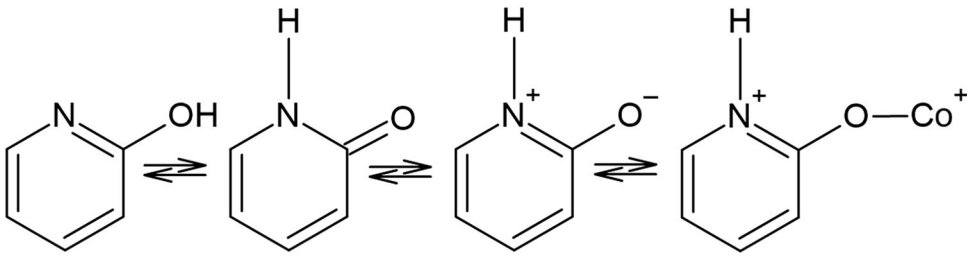

Figure 12 Pyridone tautomerism leading to the interaction of hydroxypyridine with cobalt.

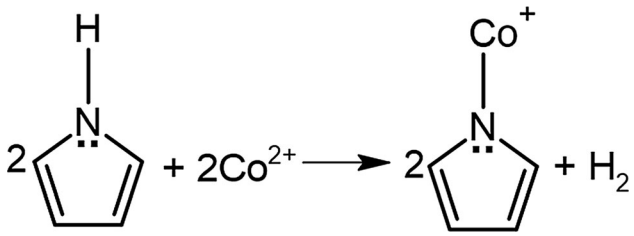

Figure 13 Interaction of pyrrole nitrogen with cobalt and the resulting formation of pyrrole-cobalt.

planes, took place, as it is shown in Fig. 11 (but very simplified). This is due to the fact, that the presence of nitrogen heteroatoms in the conjugated electronic system of the carbon matrix increases its total electron donation, thereby creating the energetic conditions, in which cobalt ions can attach directly to the aromatic ring or form complexes with individual aromatic fragments.

Pyridone and pyrrole are known to possess the properties of a weak acid; therefore, they can cause the maximum at pK_a = 7.15 (see Fig. 9). The number of these weakly acidic sites (according to Bronsted) increased by one third in the Co(20),N/AC_{ox} catalyst, and also increased by three in the Co(10),N/AC_{ox} catalyst after doping the nitrided carbon matrix with cobalt. This change in acidity can only be explained by simultaneous taking into consideration both the tautomerism and the chemical properties of pyridone (hydroxypyridine), as it shown in Fig. 12.

It is well known that strong bases are capable of converting pyrrole to the pyrril-anion, which is a highly π-excess hetero-analog of cyclopentadienyl. As in the presented work, the procedure of the nitrided carbon matrix doping with cobalt was carried out in a strongly alkaline restorative environment; apparently, the interaction of pyrrole nitrogen with cobalt was running with the formation of pyrrole-cobalt according to the scheme, as it shown in Fig. 13. That is why the pK_a maximum at 7.15 increased after the introduction of cobalt (see Fig. 9).

The maximum at pK_a = 9.45 (see Fig. 9) was referred to pyridine, which is known as a weak base. Pyridine exhibits properties characteristic for tertiary amines: it forms N-oxides (discussed above), and N-alkylpyridinium salts, as well as is capable of acting as a sigma-donor ligand. After doping with cobalt, the intensity of the pK_a = 9.45 peak decreased by two times in the case of Co(20),N/AC_{ox}, and it almost completely disappeared in the case of

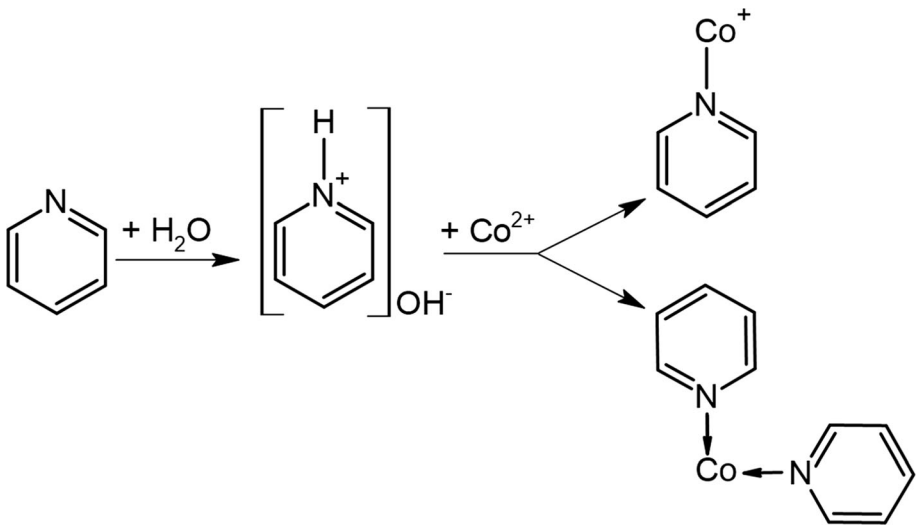

Figure 14 Chemical interaction of pyridine groups of nitrided carbon matrix and cobalt with the following formation of pyridine-cobalt, and polypyrrole-cobalt (II) complexes.

Co(10),N/AC_{ox} catalyst (see Fig. 9). It allowed to assume that the part of the introduced cobalt chemically interacted with pyridine groups, according to the mechanism of electrophilic addition at the nitrogen atom with the formation of pyridinium salts (pyridine-cobalt), as it shown in Fig. 14. Another part of the introduced cobalt participated in the formation of polypyrrole-cobalt (II) complexes, as it shown in Fig. 14 as well. It became the reason of the decreasing in the intensity of the peaks at pK^*_a = 9.45 in Fig. 9.

Conclusions

Two series of cobalt- and/or nitrogen-doped catalysts were prepared by the impregnating of pre-oxidized industrial active carbon. These were: two catalysts with 10 and 20% of cobalt content based on the oxidized active carbon, as well as two catalysts with 10 and 20% of cobalt content based on the nitrided oxidized active carbon. The presence of cobalt in all the doped samples was confirmed by both X-ray phase and X-ray structural analysis. It was found that the oxidation, nitriding, and doping with cobalt lead to the consistent decrease in the surface area and the total porosity of the original activated carbon; however, it did not affect their catalytic activity.

All the initial and synthesized doped activated carbons were investigated in the model process of sodium borohydride hydrolysis using the sealed volumometric installation at the temperature of 17 °C, as well as at higher temperatures: 60, 70, and 80 °C. It was discovered that all the doped with cobalt catalysts had significantly higher catalytic activity than the corresponding initial undoped ones. The largest amount of hydrogen released at a temperature of 17 °C was recorded on the nitrided oxidized active carbon containing 20% of cobalt. In the presence of its 0.01 g, 230 mL of H_2 released during 40 min at the hydrolysis of sodium borohydride with the initial concentration of 0.7 wt. %, which corresponded to the hydrogen generation rate of 575 mL/(g_{cat}· min). The activation energy of $NaBH_4$ hydrolysis reaction in the presence of this catalyst was 44 kJ/mole.

The largest H_2 volumes at temperatures of 60, 70, and 80 °C and hydrogen generation rates of 1667, 2857, and 5000 mL/(g_{cat}· min), respectively, were found in the presence of the catalyst doped with nitrogen and cobalt, with the content of the latter of 10%. In this case, the activation energy constituted 41 kJ/mole.

These experimental data characterize the synthesized cobalt-nitrogen-containing catalysts as highly active and competitive among the already known and well-studied catalysts that do not contain noble metals.

The study of the surface chemistry of the catalysts by the two methods (pH-potentiometric titration, and adsorption of Hammett indicators from an aqueous medium) made it possible to explain the mechanism of cobalt attachment and to determine the possible forms of its existence on the surface of the oxidized and nitrided oxidized activated carbon matrix.

The results obtained allow to recommend cobalt doped nitrogen-containing activated carbons for the preparation of highly catalytic active non-noble metal catalysts.

Funding

This study was funded by ministry of education and science of Ukraine (Grant Number No. 0120U102127).

Declarations

Conflict of interest The authors declare that they have no conflict of interest.

References

[1] Sanij FD, Balakrishnan P, Leung P, Shah A, Su H, Xu Q (2021) Advanced Pd-based nanomaterials for electro-catalytic oxygen reduction in fuel cells: a review. Int J Hydrogen Energy 46(27):14596–14627. https://doi.org/10.1016/j.ijhydene.2021.01.185

[2] Zhang L, Wang X, Zhu H (2020) Surface modifications of Pt-based atomically ordered nanoparticles to improve catalytic performances for oxygen reduction reaction. Prog Nat Sci 30(6):890–895. https://doi.org/10.1016/j.pnsc.2020.10.013

[3] Xie Y, Li Z, Liu Y, Ye Y, Zou X, Lin S (2020) Plasmon enhanced bifunctional electro-photo catalytic properties of Pt-Au/graphene composites for methanol oxidation and oxygen reduction reaction. Appl Surf Sci 508(145161):145161. https://doi.org/10.1016/j.apsusc.2019.145161

[4] Carlos Calderón J, Ndzuzo L, Bladergroen BJ, Pasupathi S (2018) Catalytic activity of carbon supported-Pt-Pd nanoparticles toward the oxygen reduction reaction. Mater Today: Proc 5(4):10551–10560. https://doi.org/10.1016/j.matpr.2017.12.387

[5] Li Q, Zhang S, Xuan W, Zhou H, Tian W, Deng X et al (2021) Microbial synthesis of highly dispersed nano-Pd electrocatalyst for oxygen reduction reaction. Int J Hydrogen Energy 46(53):26886–26896. https://doi.org/10.1016/j.ijhydene.2021.05.163

[6] Braesch G, Bonnefont A, Martin V, Savinova ER, Chatenet M (2018) Borohydride oxidation reaction mechanisms and poisoning effects on Au, Pt and Pd bulk electrodes: From model (low) to direct borohydride fuel cell operating (high) concentrations. Electrochim Acta 273:483–494. https://doi.org/10.1016/j.electacta.2018.04.068

[7] Martins M, Šljukić B, Sequeira CAC, Metin Ö, Erdem M, Sener T et al (2016) Biobased carbon-supported palladium electrocatalysts for borohydride fuel cells. Int J Hydrogen Energy 41(25):10914–10922. https://doi.org/10.1016/j.ijhydene.2016.04.039

[8] Oliveira RCP, Milikić J, Daş E, Yurtcan AB, Santos DMF, Šljukić B (2018) Platinum/polypyrrole-carbon electrocatalysts for direct borohydride-peroxide fuel cells. Appl Catal B 238:454–464. https://doi.org/10.1016/j.apcatb.2018.06.057

[9] Kadioglu T, Turkmen AC, Ata KC, Akay RG, Tikiz I, Celik C (2020) Investigation of the performance of a direct borohydride fuel cell with low Pt/C catalyst loading under different operating conditions. Int J Hydrogen Energy 45(60):35006–35012. https://doi.org/10.1016/j.ijhydene.2020.08.176

[10] Li H, Liao J, Zhang X, Liao W, Wen L, Yang J et al (2013) Controlled synthesis of nanostructured Co film catalysts with high performance for hydrogen generation from sodium borohydride solution. J Power Sources 239:277–283. https://doi.org/10.1016/j.jpowsour.2013.03.167

[11] Chen Y, Wang S, Li Z (2020) A cobalt–pyrrole coordination compound as high performance cathode catalyst for direct borohydride fuel cells. RSC Adv 10(49):29119–29127. https://doi.org/10.1039/d0ra05143h

[12] Lu A, Chen Y, Jin J, Yue G-H, Peng D-L (2012) CoO nanocrystals as a highly active catalyst for the generation of hydrogen from hydrolysis of sodium borohydride. J Power Sources 220:391–398. https://doi.org/10.1016/j.jpowsour.2012.08.010

[13] Kılınç D, Şahin Ö, Saka C (2017) Investigation on salisylaldimine-Ni complex catalyst as an alternative to increasing the performance of catalytic hydrolysis of sodium borohydride. Int J Hydrogen Energy 42(32):20625–20637. https://doi.org/10.1016/j.ijhydene.2017.06.230

[14] Ekinci A, Cengiz E, Kuncan M, Şahin Ö (2020) Hydrolysis of sodium borohydride solutions both in the presence of Ni–B catalyst and in the case of microwave application. Int J Hydrogen Energy 45(60):34749–34760. https://doi.org/10.1016/j.ijhydene.2020.08.264

[15] Li ZP, Ma SL, Li GR, Liu BH (2013) Hydrogen generation from borohydride hydrolysis on surface-alloyed Ni foam. J Power Sources 242:621–626. https://doi.org/10.1016/j.jpowsour.2013.05.103

[16] Duman S, Kaya B, Caf F, Enez B, Fincan SA (2021) Innovative hydrogen release from sodium borohydride hydrolysis using biocatalyst-like Fe_2O_3 nanoparticles impregnated on Bacillus simplex bacteria. Int J Hydrogen Energy 46(29):15410–15430. https://doi.org/10.1016/j.ijhydene.2021.02.028

[17] Nabid MR, Bide Y, Kamali B (2019) Hydrogen release from sodium borohydride by Fe_2O_3@nitrogen-doped carbon core-shell nanosheets as reasonable heterogeneous catalyst. Int J Hydrogen Energy 44(47):25662–25670. https://doi.org/10.1016/j.ijhydene.2019.08.038

[18] Ocon JD, Tuan TN, Yi Y, de Leon RL, Lee JK, Lee J (2013) Ultrafast and stable hydrogen generation from sodium borohydride in methanol and water over Fe–B nanoparticles. J Power Sources 243:444–450. https://doi.org/10.1016/j.jpowsour.2013.06.019

[19] Kassem AA, Abdelhamid HN, Fouad DM, Ibrahim SA (2019) Metal-organic frameworks (MOFs) and MOFs-derived CuO@C for hydrogen generation from sodium borohydride. Int J Hydrogen Energy 44(59):31230–31238. https://doi.org/10.1016/j.ijhydene.2019.10.047

[20] Chinnappan A, Puguan JMC, Chung W-J, Kim H (2015) Hydrogen generation from the hydrolysis of sodium borohydride using chemically modified multiwalled carbon nanotubes with pyridinium based ionic liquid and decorated with highly dispersed Mn nanoparticles. J Power Sources 293:429–436. https://doi.org/10.1016/j.jpowsour.2015.05.096

[21] Wang H, Ding J, Kannan P, Subramanian P, Ji S (2021) MnOOH nanoparticles integrated nitrogen doped porous nanosheet-like carbon network as a non-noble catalyst for electro-oxidation of sodium borohydride. Int J Hydrogen Energy 46(14):9380–9393. https://doi.org/10.1016/j.ijhydene.2020.12.082

[22] Sun R-M, Yao Y-Q, Wang A-J, Fang K-M, Zhang L, Feng J-J (2021) One-step pyrolysis synthesis of nitrogen, manganese-codoped porous carbon encapsulated cobalt-iron nanoparticles with superior catalytic activity for oxygen reduction reaction. J Colloid Interface Sci 592:405–415. https://doi.org/10.1016/j.jcis.2021.02.071

[23] Liu Y, Wen H, Zhou D, Huang X, Wu X, Jiang J et al (2021) Tuning surface d charge of Ni-Ru alloys for unprecedented catalytic activity towards hydrogen generation from ammonia borane hydrolysis. Appl Catal B 291(120094):120094. https://doi.org/10.1016/j.apcatb.2021.120094

[24] Loghmani MH, Shojaei AF, Khakzad M (2017) Hydrogen generation as a clean energy through hydrolysis of sodium borohydride over Cu-Fe-B nano powders: Effect of polymers and surfactants. Energy (Oxf) 126:830–840. https://doi.org/10.1016/j.energy.2017.03.006

[25] Paksoy A, Kurtoğlu SF, Dizaji AK, Altıntaş Z, Khoshsima S, Uzun A et al (2021) Nanocrystalline cobalt–nickel–boron (metal boride) catalysts for efficient hydrogen production from the hydrolysis of sodium borohydride. Int J Hydrogen Energy 46(11):7974–7988. https://doi.org/10.1016/j.ijhydene.2020.12.017

[26] Liang Z, Xiao X, Yu X, Huang X, Jiang Y, Fan X et al (2018) Non-noble trimetallic Cu-Ni-Co nanoparticles supported on metal-organic frameworks as highly efficient catalysts for hydrolysis of ammonia borane. J Alloys Compd 741:501–508. https://doi.org/10.1016/j.jallcom.2017.12.151

[27] Bogdanovskaya V, Vernigor I, Radina M, Andreev V, Korchagin O (2021) Nanocomposite cathode catalysts containing platinum deposited on carbon nanotubes modified by O, N, and P atoms. Catalysts 11(3):335. https://doi.org/10.3390/catal11030335

[28] Ivanenko I, Voronova A, Astrelin I, Romanenko Y (2019) Structural and catalytic properties of Ni–Co spinel and its composites. Bull Mater Sci 42(4):172. https://doi.org/10.1007/s12034-019-1854-9

[29] Zhang H, Xu G, Zhang L, Wang W, Miao W, Chen K et al (2020) Ultrafine cobalt nanoparticles supported on carbon nanospheres for hydrolysis of sodium borohydride. Renew Energy 162:345–354. https://doi.org/10.1016/j.renene.2020.08.031

[30] Zhang H, Zhang L, Rodríguez-Pérez IA, Miao W, Chen K, Wang W et al (2021) Carbon nanospheres supported bimetallic Pt-Co as an efficient catalyst for $NaBH_4$ hydrolysis. Appl Surf Sci 540(148296):148296. https://doi.org/10.1016/j.apsusc.2020.148296

[31] Saka C, Salih Eygi M, Balbay A (2020) CoB doped acid modified zeolite catalyst for enhanced hydrogen release from sodium borohydride hydrolysis. Int J Hydrogen Energy 45(30):15086–15099. https://doi.org/10.1016/j.ijhydene.2020.03.238

[32] Zahmakıran M, Ayvalı T, Akbayrak S, Çalışkan S, Çelik D, Özkar S (2011) Zeolite framework stabilized nickel(0) nanoparticles: active and long-lived catalyst for hydrogen generation from the hydrolysis of ammonia-borane and sodium borohydride. Catal Today 170(1):76–84. https://doi.org/10.1016/j.cattod.2010.09.022

[33] Kıpçak İ, Kalpazan E (2020) Preparation of CoB catalysts supported on raw and Na-exchanged bentonite clays and their application in hydrogen generation from the hydrolysis of $NaBH_4$. Int J Hydrogen Energy [Internet], Available from: Doi: https://doi.org/10.1016/j.ijhydene.2020.03.230

[34] Cui Z, Guo Y, Ma J (2016) In situ synthesis of graphene supported Co-Sn-B alloy as an efficient catalyst for hydrogen generation from sodium borohydride hydrolysis. Int J Hydrogen Energy 41(3):1592–1599. https://doi.org/10.1016/j.ijhydene.2015.11.081

[35] Li B, Yan Q, Song C, Yan P, Ye K, Cheng K et al (2019) Reduced graphene oxide foam supported CoNi nanosheets as an efficient anode catalyst for direct borohydride hydrogen peroxide fuel cell. Appl Surf Sci 491:659–669. https://doi.org/10.1016/j.apsusc.2019.06.110

[36] Wei Y, Huang X, Wang J, Yu H, Zhao X, Cheng D (2017) Synthesis of bifunctional non-noble monolithic catalyst Co-W-P/carbon cloth for sodium borohydride hydrolysis and reduction of 4-nitrophenol. Int J Hydrogen Energy 42(41):25860–25868. https://doi.org/10.1016/j.ijhydene.2017.08.148

[37] Peng C, Li T, Zou Y, Xiang C, Xu F, Zhang J et al (2021) Bacterial cellulose derived carbon as a support for catalytically active Co–B alloy for hydrolysis of sodium borohydride. Int J Hydrogen Energy 46(1):666–675. https://doi.org/10.1016/j.ijhydene.2020.10.026

[38] Sahiner N, Seven F (2014) The use of superporous p(AAc (acrylic acid)) cryogels as support for Co and Ni nanoparticle preparation and as reactor in H_2 production from sodium borohydride hydrolysis. Energy (Oxf) 71:170–179. https://doi.org/10.1016/j.energy.2014.04.031

[39] Ai L, Gao X, Jiang J (2014) In situ synthesis of cobalt stabilized on macroscopic biopolymer hydrogel as economical and recyclable catalyst for hydrogen generation from sodium borohydride hydrolysis. J Power Sources 257:213–220. https://doi.org/10.1016/j.jpowsour.2014.01.119

[40] Marchionni A, Bevilacqua M, Filippi J, Folliero MG, Innocenti M, Lavacchi A et al (2015) High volume hydrogen production from the hydrolysis of sodium borohydride using a cobalt catalyst supported on a honeycomb matrix. J Power Sources 299:391–397. https://doi.org/10.1016/j.jpowsour.2015.09.006

[41] Zhuang D-W, Dai H-B, Zhong Y-J, Sun L-X, Wang P (2015) A new reactivation method towards deactivation of honeycomb ceramic monolith supported cobalt–molybdenum–boron catalyst in hydrolysis of sodium borohydride. Int J

Hydrogen Energy 40(30):9373–9381. https://doi.org/10.1016/j.ijhydene.2015.05.177

[42] Strelko VV, Kartel NT, Dukhno IN, Kuts VS, Clarkson RB, Odintsov BM (2004) Mechanism of reductive oxygen adsorption on active carbons with various surface chemistry. Surf Sci 548(1–3):281–290. https://doi.org/10.1016/j.susc.2003.11.012

[43] Bagreev A, Menendez JA, Dukhno I, Tarasenko Y, Bandosz TJ (2005) Oxidative adsorption of methyl mercaptan on nitrogen-enriched bituminous coal-based activated carbon. Carbon N Y 43(1):208–210. https://doi.org/10.1016/j.carbon.2004.09.003

[44] Yuan X, Li L, Ma Z, Yu X, Wen X, Ma Z-F et al (2016) Novel nanowire-structured polypyrrole-cobalt composite as efficient catalyst for oxygen reduction reaction. Sci Rep 6(1):20005. https://doi.org/10.1038/srep20005

[45] Wang H, Ma N, Yan Z, Deng L, He J, Hou Y et al (2015) Cobalt/polypyrrole nanocomposites with controllable electromagnetic properties. Nanoscale 7(16):7189–7196. https://doi.org/10.1039/c4nr06978a

[46] Chou C-C, Hsieh C-H, Chen B-H (2015) Hydrogen generation from catalytic hydrolysis of sodium borohydride using bimetallic Ni–Co nanoparticles on reduced graphene oxide as catalysts. Energy (Oxf) 90:1973–1982. https://doi.org/10.1016/j.energy.2015.07.023

[47] Zhu YM, Zhao CL, Xu YL, Hu CS, Zhao XF (2019) Preparation and characterization of coal pitch-based needle coke (Part I): the effects of aromatic index (f_a) in refined coal pitch. Energy Fuel 33(4):3456–3464. https://doi.org/10.1021/acs.energyfuels.9b00160

[48] Zhu YM, Hu CS, Xu YL, Zhao CL, Yin XT, Zhao XF (2020) Preparation and characterization of coal pitch-based needle coke (part II): the effects of β resin in refined coal pitch. Energy Fuel 34(2):2126–2134. https://doi.org/10.1021/acs.energyfuels.9b03406

[49] Zhu YM, Liu HM, Xu YL et al (2020) Preparation and characterization of coal-pitch-based needle coke (part III): the effects of quinoline insoluble in coal tar pitch. Energy Fuel 34(7):8676–8684. https://doi.org/10.1021/acs.energyfuels.0c01049

[50] Han X, Lin H, Zheng Y (2015) The role of oxygen functional groups in the adsorption of heteroaromatic nitrogen compounds. J Hazard Mater 297:217–223. https://doi.org/10.1016/j.jhazmat.2015.04.056

[51] Jaramillo J, Álvarez PM, Gómez-Serrano V (2010) Oxidation of activated carbon by dry and wet methods. Fuel Process Technol 91(11):1768–1775. https://doi.org/10.1016/j.fuproc.2010.07.018

[52] Akti F (2021) Hydrogen generation from hydrolysis of sodium borohydride by silica xerogel supported cobalt catalysts: Positive roles of amine modification and calcination treatment. Fuel (Lond) 303(121326):121326. https://doi.org/10.1016/j.fuel.2021.121326

[53] Soltani M, Zabihi M (2020) Hydrogen generation by catalytic hydrolysis of sodium borohydride using the nano-bimetallic catalysts supported on the core-shell magnetic nanocomposite of activated carbon. Int J Hydrogen Energy [Internet]. Available from: Doi: https://doi.org/10.1016/j.ijhydene.2020.02.203

[54] Balbay A, Selvitepe N, Saka C (2021) Fe doped-CoB catalysts with phosphoric acid-activated montmorillonite as support for efficient hydrogen production via $NaBH_4$ hydrolysis. Int J Hydrogen Energy 46(1):425–438. https://doi.org/10.1016/j.ijhydene.2020.09.181

[55] Li Z, Xu Y, Guo Q, Li Y, Ma X, Li B et al (2021) Preparation of Ag@PNCMs nanocomposite as an effective catalyst for hydrogen generation from hydrolysis of sodium borohydride. Mater Lett 297(129828):129828. https://doi.org/10.1016/j.matlet.2021.129828

[56] Didehban A, Zabihi M, Babajani N (2020) Preparation of the efficient nano-bimetallic cobalt-nickel catalysts supported on the various magnetic substrates for hydrogen generation from hydrolysis of sodium borohydride in alkaline solutions. Polyhedron 180(114405):114405. https://doi.org/10.1016/j.poly.2020.114405

[57] Balčiūnaitė A, Sukackienė Z, Antanavičiūtė K, Vaičiūnienė J, Naujokaitis A, Tamašauskaitė-Tamašiūnaitė L et al (2021) Investigation of hydrogen generation from sodium borohydride using different cobalt catalysts. Int J Hydrogen Energy 46(2):1989–1996. https://doi.org/10.1016/j.ijhydene.2020.10.047

[58] Wang X, Liao J, Li H, Wang H, Wang R, Pollet BG et al (2018) Highly active porous Co–B nanoalloy synthesized on liquid-gas interface for hydrolysis of sodium borohydride. Int J Hydrogen Energy 43(37):17543–17555. https://doi.org/10.1016/j.ijhydene.2018.07.147

[59] Rambabu K, Hai A, Bharath G, Banat F, Show PL (2019) Molybdenum disulfide decorated palm oil waste activated carbon as an efficient catalyst for hydrogen generation by sodium borohydride hydrolysis. Int J Hydrogen Energy 44(28):14406–14415. https://doi.org/10.1016/j.ijhydene.2019.03.085

[60] Fangaj E, Ceyhan AA (2020) Apricot Kernel shell waste treated with phosphoric acid used as a green, metal-free catalyst for hydrogen generation from hydrolysis of sodium borohydride. Int J Hydrogen Energy 45(35):17104–17117. https://doi.org/10.1016/j.ijhydene.2020.04.133

[61] Abdelhamid HN (2021) A review on hydrogen generation from the hydrolysis of sodium borohydride. Int J Hydrogen

Energy 46(1):726–765. https://doi.org/10.1016/j.ijhydene.2020.09.186

[62] Bandosz TJ, Jagiełło J, Schwarz JA, Krzyzanowski A (1996) Effect of surface chemistry on sorption of water and methanol on activated carbons. Langmuir 12(26):6480–6486. https://doi.org/10.1021/la960340r